frontiers | Frontiers in Physics

TYPE Original Research
PUBLISHED 21 November 2022
DOI 10.3389/fphy.2022.1084214

OPEN ACCESS

EDITED BY
Ye Yuan,
Songshan Lake Material Laboratory,
China

REVIEWED BY
Liuan Li,
Jilin University, China
Liang He,
No.5 Electronics Research Institute of the Ministry of Industry and Information Technology, China

*CORRESPONDENCE
Baijun Zhang,
zhbaij@mail.sysu.edu.cn

SPECIALTY SECTION
This article was submitted to Interdisciplinary Physics, a section of the journal Frontiers in Physics

RECEIVED 30 October 2022
ACCEPTED 11 November 2022
PUBLISHED 21 November 2022

CITATION
Liu H, Liang Z, Wang F, Xu Y, Yang X, Liang Y, Li X, Lin L, Wu Z, Liu Y and Zhang B (2022), Analysis of electrical properties in lateral Schottky barrier diode based on n-GaN and AlGaN/GaN heterostructure.
Front. Phys. 10:1084214.
doi: 10.3389/fphy.2022.1084214

Analysis of electrical properties in lateral Schottky barrier diode based on n-GaN and AlGaN/GaN heterostructure

Honghui Liu, Zhiwen Liang, Fengge Wang, Yanyan Xu, Xien Yang, Yisheng Liang, Xin Li, Lizhang Lin, Zhisheng Wu, Yang Liu and Baijun Zhang*

State Key Laboratory of Optoelectronic Materials and Technologies, School of Electronics and Information Technology, Sun Yat-sen University, Guangzhou, China

In this paper, the lateral Schottky barrier diodes (SBDs) with small capacitance and low turn-on voltage (V_{on}) were fabricated on n-GaN and AlGaN/GaN heterostructure. The capacitances of lateral n-GaN SBD and lateral AlGaN/GaN SBD are 1.35 pF/mm and 0.70 pF/mm, respectively. Compared with the planar SBDs, the capacitances of lateral SBDs are reduced by about two orders of magnitude without sacrificing the performance of on-resistance (R_{on}) and reverse leakage current. For the planar and lateral n-GaN SBDs, the value of the V_{on} is similar. However, compared with the planar AlGaN/GaN SBD, the V_{on} of lateral AlGaN/GaN SBD is reduced from 1.64 V to 0.87 V owing to the anode metal directly contacting the two-dimensional electron gas. According to temperature-dependent *I-V* results, the barrier inhomogeneity of the lateral SBD is more intensive than the planar SBD, which is attributed to etching damage. The withstand voltage of SBD is a very important parameter for power electronic applications. Compared with the breakdown voltage of 73 V in the lateral n-GaN SBD, the lateral AlGaN/GaN SBDs exhibit a breakdown voltage of 2322 V. In addition, we found that Schottky contact introduces anode resistance (R_A) by analysing the R_{on} distribution of lateral SBDs. The experimental results also show that the R_A of lateral n-GaN SBD and lateral AlGaN/GaN SBD are 10.5 Ω mm and 9.2 Ω mm respectively, which are much larger than the ohmic contact resistance due to worsening anode contact by metal-induced gap states.

KEYWORDS

GaN, AlGaN/GaN, Schottky barrier diodes, metal-induced gap states, inhomogeneous SBHs

10.3389/fphy.2022.1084214

Introduction

GaN-based Schottky barrier diodes (SBDs) exhibit outstanding power handling capabilities in power electronic applications [1, 2] and multipliers [3] due to the physical properties of wide bandgap and high breakdown electric field [4–6]. In particular, AlGaN/GaN SBDs exhibit excellent characteristics of high electron mobility and high electron density due to the 2D electron gas (2DEG) [7, 8], offering wide applications for high-frequency and high-power devices [9, 10]. SBD is one of the most essential components in microwave power transmission systems [3, 10–12]. However, the high-frequency performance of SBD requires low turn-on voltage (V_{on}) to reduce conduction loss, and high cut-off frequency to improve operating frequency. In addition, the cut-off frequency of SBD is limited by the product of capacitance and the on-resistance (R_{on}), hence reducing the anode size cannot effectively improve the cut-off frequency. Conventional planar AlGaN/GaN SBDs have undesirable high V_{on} and large capacitance. The metals (TiN, Mo, and W) of the low Schottky barrier can reduce V_{on}, which are accompanied by a higher reverse leakage current (J_r) [13–15]. The recessed anode structure is an effective solution to avoid these two shortages because the 2DEG directly contacts the anode metal [16, 17]. Even so, this design still has a large capacitance due to the parallel plate capacitor caused by the anode field plate (FP) and 2DEG [18, 19]. Compared with the SBD of the recessed anode structure, the capacitance of the lateral SBD can be further reduced. Moreover, the lateral GaN-based SBDs also have low V_{on} because the carriers directly contact the anode metal. Many researchers have reported studies about the transport mechanism [16, 20, 21], Schottky barrier heights (SBHs) [22, 23], metal-induced gap states (MIGS) [24–26], and barrier inhomogeneity [27–30] on planar n-GaN SBDs or AlGaN/GaN recessed-SBDs. Nevertheless, the electrical properties in lateral GaN-based SBDs are rarely reported.

In this paper, the strategy of lateral GaN-based SBDs was used to eliminate the FP capacitance and reduce V_{on} without sacrificing the performance of R_{on} and reverse leakage. The simulated results show the characteristics of the energy band and carrier distribution. The analysis of electrical properties in lateral GaN-based SBDs was described by current-voltage (I-V) and capacitance-voltage (C-V) characteristics. According to the results of temperature-dependent I-V measurements, the barrier inhomogeneity of the lateral SBDs is more intensive than that of planar SBDs, which is attributed to etching damage. In addition, anode resistance (R_A) was present, which is possibly due to the worsening anode contacts by MIGS.

Experimental details

The lateral GaN-based SBDs in this study were fabricated on n-GaN and AlGaN/GaN heterostructure and were shown in Figure 1A. The wafers were grown by metal-organic chemical vapor deposition (MOCVD) on 2-inch c-sapphire substrates. The epitaxial layers consist of a ~40 nm-thick AlN, a 4 μm-thick high resistive (HR) GaN buffer layer, and a 300 nm-thick i-GaN. Based on this template, the n-GaN and AlGaN/GaN heterostructure continued to grow 500 nm-thick n-GaN and 24/0.7 nm-thick $Al_{0.25}Ga_{0.75}N$/AlN, respectively. The electron mobility, electron density, and channel thickness of n-GaN and AlGaN/GaN are summarized in Table 1. The ring cathode metals (Ti/Al/Ni/Au = 20/150/50/80 nm) were deposited on the wafer surface by E-beam evaporation and annealed at 850°C for 30 s in N_2 ambient. Using the transfer length method (TLM), the ohmic contact resistances (R_C) of n-GaN and AlGaN/GaN are 0.65 Ω mm and 1.13 Ω mm, respectively. The anode metals (Ni/Au = 50/80 nm) were deposited on the wafer surface. Figure 1B shows the cross-sectional schematic of the fabricated planar SBD. For lateral SBD, the anode region was etched to the HR GaN buffer layer by inductively coupled plasma (ICP), followed by direct deposition of anode metal to the sidewall, as shown in Figure 1C. The diameter of the circular anode metal was 200 μm. The distance between the anode metal and the ring cathode metal was 40 μm. The I-V and C-V characteristics were measured by the Agilent B1500A at room temperature.

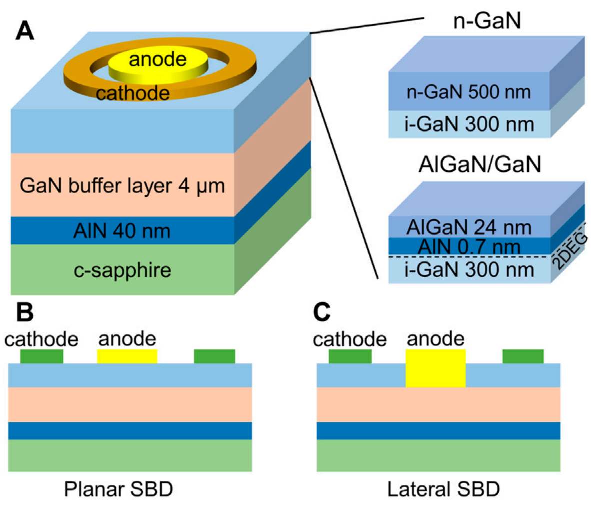

FIGURE 1
(A) Schematic illustrations of n-GaN and AlGaN/GaN SBDs with epitaxial information. The schematic cross-section of **(B)** planar and **(C)** lateral SBDs.

Results and discussion

According to the n-GaN and AlGaN/GaN SBDs structures, the characteristics of the energy band and carrier distribution are

TABLE 1 The key material parameters of n-GaN and AlGaN/GaN.

	Electron density (cm^{-3})	Electron mobility (cm^2/Vs.)	Channel thickness (nm)	R_{sh} (Ω/□)
n-GaN	3.4×10^{17}	448	500	786
AlGaN/GaN	3.4×10^{19}	1969	~2.8	306

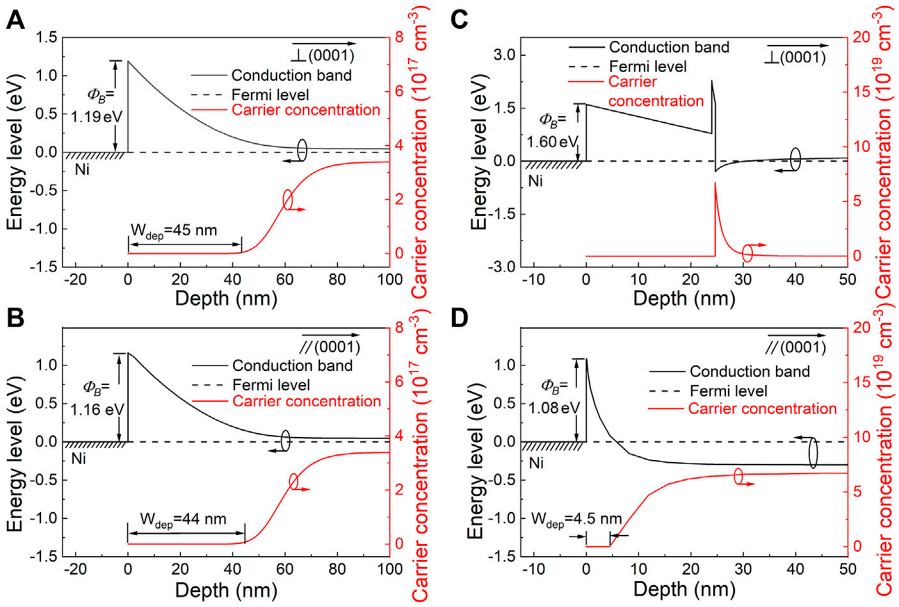

FIGURE 2
The energy band and carrier distribution of **(A)** planar n-GaN SBD, **(B)** lateral n-GaN SBD, **(C)** planar AlGaN/GaN SBD, and **(D)** lateral AlGaN/GaN SBD at 0 V.

simulated by Synopsys' Sentaurus technology computer-aided design (TCAD), and the results are shown in Figure 2. The depletion directions of the planar and lateral SBDs are perpendicular and parallel to the (0,001) plane, respectively. The energy band and carrier distribution are very similar between planar and lateral n-GaN SBDs because both are Ni/n-GaN contacts. The simulation results show that the sample with SBH of about 1.18 eV has a depletion width of about 44.5 nm for n-GaN with doping concentration of 3.4×10^{17} cm^{-3}, as shown in Figures 2A,B. However, the energy band structures of the planar and lateral AlGaN/GaN SBDs are very different, as shown in Figures 2C,D. The energy band structure of the planar AlGaN/GaN SBD displays that anode metal cannot deplete the 2DEG channel at 0 V, and its SBH is 1.60 eV. The 2DEG is distributed in the i-GaN layer of the AlGaN/GaN heterostructure, which is only a ~2.8 nm-thick sheet channel. The simulation results of the energy band and carrier distribution of the lateral AlGaN/GaN SBD are shown in Figure 2D. For lateral AlGaN/GaN SBD, the lateral contact of Ni-2DEG can be treated as SBD of a heavily doped n^+-GaN sheet channel. The Ni-2DEG forms a SBH of 1.08 eV, which only depletes 4.5 nm 2DEG.

As shown in Figures 3A–H, we measured the *I-V* and *C-V* characteristics of each SBD at different temperatures from 298 to 504 K. The *I-V* and *C-V* curves conform to traditional SBD depletion characteristics for planar n-GaN SBD, lateral n-GaN SBD, and lateral AlGaN/GaN SBD. However, the *I-V* and *C-V* curves of the planar AlGaN/GaN SBD are different from the characteristics of traditional SBD depletion. Because anode metal and 2DEG channel are separated by AlGaN barrier layer. The V_{on} of the planar AlGaN/GaN SBD is as high as 1.64 V since the device conduction requires electrons to pass through the AlGaN barrier layer, while the other three devices show very low V_{on} because electrons only need to overcome the barriers to flow to the anode. The J_r of the planar AlGaN/GaN SBD reaches saturation at pinch-off voltage (-4.2 V) due to 2DEG depletion, as shown in Figure 3C. The capacitance characteristic of planar AlGaN/GaN SBD is fitted to the parallel plate capacitor model of the anode metal and 2DEG [18]. At lower reverse bias voltage, the planar AlGaN/GaN SBD

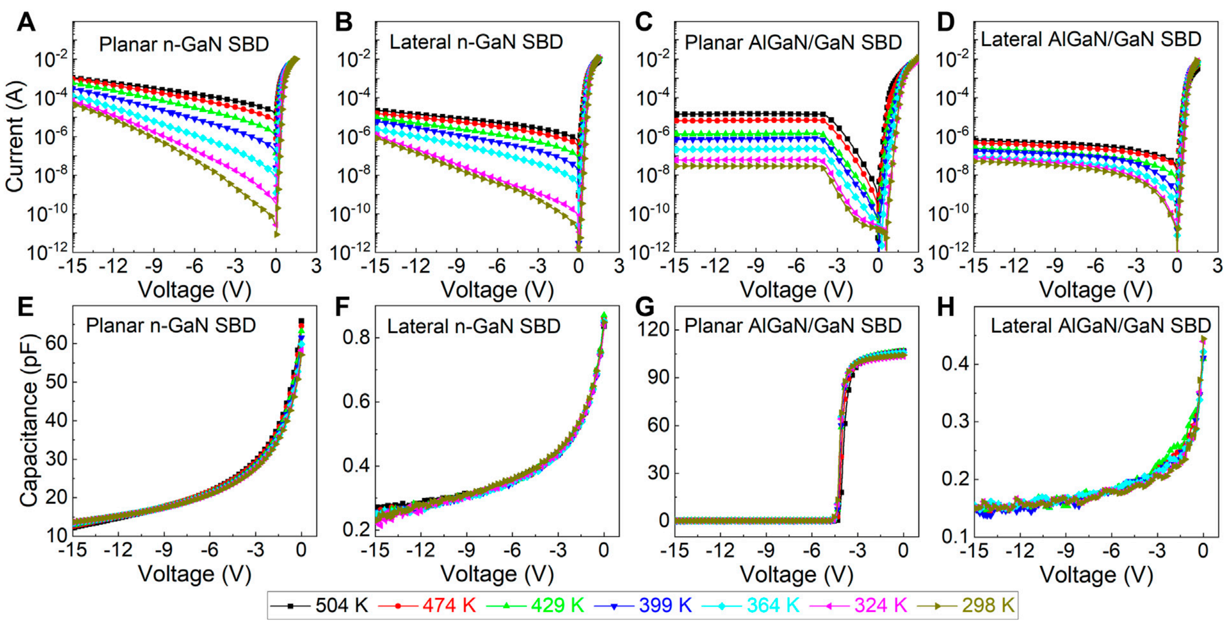

FIGURE 3
The *I-V* **(A–D)** and *C-V* **(E–H)** characteristics of planar n-GaN SBD, lateral n-GaN SBD, planar AlGaN/GaN SBD, and lateral AlGaN/GaN SBD at temperatures of 504 K, 474 K, 429 K, 399 K, 364 K, 324 K and 298 K.

maintains a stable capacitance value due to the characteristics of parallel plate capacitors. With increasing reverse bias voltage, the 2DEG is gradually depleted, which causes the capacitance to drop rapidly due to the disappearance of the plate capacitor. At higher reverse bias voltage, the capacitance tends to zero, the 2DEG is completely depleted, as shown in Figure 3G. The capacitance approaching zero also shows the HR characteristics of the buffer layer. The n-GaN and AlGaN/GaN SBDs of different FP widths are measured, the values of zero bias capacitance are linear with the area of the FP, so the lateral SBD without FP can effectively eliminate the FP capacitance. Compared with the planar SBDs, the capacitances of the lateral SBDs are reduced by two orders of magnitude without sacrificing the performance of the R_{on} and J_r. This is attributed to two characteristics of lateral SBDs: the small anode area and the elimination of spreading resistance under the anode metal. The capacitances of lateral n-GaN SBD and lateral AlGaN/GaN SBD are 1.35 pF/mm and 0.70 pF/mm, respectively.

In order to extract the SBH Φ_B, the ideality factor n, and the R_{on} from the *I-V* curve, the thermionic emission (TE) can be described as the major forward current contribution [28, 31],

$$I = AA^*T^2 \exp\left(\frac{-q\Phi_B}{kT}\right)\left\{\exp\left[\frac{q(V - IR_{on})}{nkT}\right] - 1\right\} \tag{1}$$

where A is the area of the anode metal, A^* is the effective Richardson constant (226.4 $\mathrm{Acm^{-2}K^{-2}}$), k is the Boltzmann constant, and T is the temperature. From the *I-V* and *C-V* curves at room temperature, the device parameters of each SBD are summarized in Table 2. The SBHs extracted by the *I-V* characteristics are lower than the simulation results, which may be due to electron tunneling and inhomogeneity SBHs [27–29]. The ideality factors of each SBD are larger than 1, which indicates that in addition to TE, other transport mechanisms include thermionic field emission (TFE) and field emission (FE) [32, 33]. For planar AlGaN/GaN SBD, the ideality factor of ~2 illustrates the existence of various transport types other than TE, such as trap-assisted tunneling (TAT) and recombination [34].

The ideality factors of each SBD are extracted from the *I-V* curve at different temperatures and shown in Figure 4A, which are larger than 1. Hence, the transport mechanism includes other mechanisms other than TE. What's more, TE is more sensitive to temperature, and the ideality factors are positively related to 1,000/T due to the domination of the TE mechanism at high temperatures.

Figure 4B shows SBHs for each SBD at temperatures ranging from 298 to 504 K. The SBHs of each SBD were extracted from the forward *I-V* curves by Eq. 1. The SBHs decrease with increasing 1,000/T due to the inhomogeneous nature of the barrier. The electrons only overcome lower barriers at lower temperatures. With increasing temperature, the energy of the electrons increases to overcome the higher barriers at the Ni/GaN interface, where the higher SBHs were exhibited. The inhomogeneous SBHs can be expressed as a Gaussian

TABLE 2 The electrical characteristics of n-GaN SBDs and AlGaN/GaN SBDs at room temperature.

	n-GaN		AlGaN/GaN	
	Planar SBD	Lateral SBD	Planar SBD	Lateral SBD
V_{on} (V)	0.72	0.83	1.64	0.87
Capacitance at 0 V (pF)	65.89	0.85	104.24	0.44
Leakage current at -15 V (A)	4.79×10^{-5}	8.54×10^{-7}	2.88×10^{-8}	2.27×10^{-7}
$SBH_{(I-V)}$ (eV)	0.83	0.91	1.15	0.84
$SBH_{(simulated)}$ (eV)	1.19	1.16	1.60	1.08
Ideality factor	1.21	1.34	1.99	1.58
R_{on} (Ω)	55.1	32.9	62.4	59.5
R_A (Ω·mm)	12.3	10.5	23.1	9.16

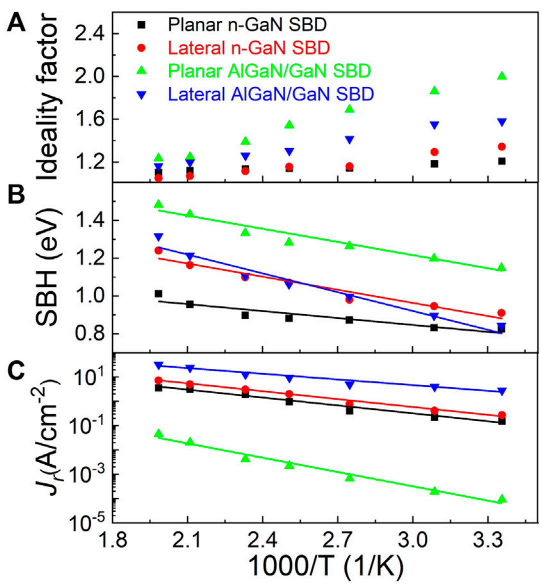

FIGURE 4
(A) Ideality factor, (B) barrier height, and (C) J_r as a dependence of 1,000/T for each SBD device.

distribution with a mean barrier height $\overline{\Phi_{B0}}$ and a standard deviation σ, as shown in Eq. 2 [30].

$$\Phi_B(T) = \overline{\Phi_{B0}} - \frac{\sigma^2}{2kT} \tag{2}$$

In GaN-based SBDs, inhomogeneous SBHs are attributed to multiple factors such as material defects, interface dipole layers, morphological features, and surface Fermi level pinning [27–30, 35]. According to the linear fits of the SBHs vs 1,000/T curve, the values of σ were estimated to be 145, 199, 200 and 239 meV for planar n-GaN SBD, lateral n-GaN SBD, planar AlGaN/GaN SBD and lateral AlGaN/GaN SBD, respectively. Compared to the planar SBDs, the lateral SBDs exhibit larger σ may be due to the etching damage caused by ICP. The lateral AlGaN/GaN SBD has the largest σ value, which is attributed to the higher trap concentration at the contact of anode metal and 2DEG. Thermal annealing is an effective step to reduce the damages induced by ICP etching, and wet treatment methods are used to further treat etching damage, such as hydroxide (KOH) and $(NH_4)_2S$ [36, 37].

At the voltage of -15 V, the J_r vs 1,000/T (J_r-T) characteristics are shown in Figure 4C, which appears linear on the Arrhenius plot. This suggests that the thermal activation mechanism has a dependence on the exp $(-E_A/kT)$ function, where E_A is the activation energy. Therefore, a possible reverse leakage mechanism is defined as TAT, which is associated with thermally activated current [38]. The values of E_A were estimated to be 215, 214, 387 and 156 meV for planar n-GaN SBD, lateral n-GaN SBD, planar AlGaN/GaN SBD, and lateral AlGaN/GaN SBD, respectively, according to linear fitting J_r-T data. In addition, the J_r is related to the trap concentration on the interface of anode metal and semiconductor.

The withstand voltage of SBD is a very important parameter for power electronic applications. The reverse breakdown voltages of these SBDs are shown in Figure 5. The planar n-GaN SBD has no breakdown phenomenon at -28.5 V. The lateral n-GaN SBD shows a relatively low leakage current, which is breakdown at -73 V. Compared with n-GaN SBD, the AlGaN/GaN SBDs exhibit a breakdown voltage of more than 2300 V, which is mainly attributed to the undoped AlGaN/GaN materials.

For planar and lateral SBDs, the R_{on} consists of the R_C, channel resistance ($R_{channel}$) and anode resistance (R_A). Using the TLM, we calculated the R_C and $R_{channel}$ for each SBD. Unitized R_{on} distributions of each SBD are summarized in Figure 6A. The experimental results show that the R_A of lateral n-GaN SBD and lateral AlGaN/GaN SBD are 10.5 Ω mm and 9.2 Ω mm, respectively. The R_A are much larger than the R_C in each SBD, which is probably due to the worsening anode contacts by MIGS. The energy diagram of n-GaN SBD with MIGS is displayed in Figure 6B. The planar AlGaN/GaN SBD exhibits

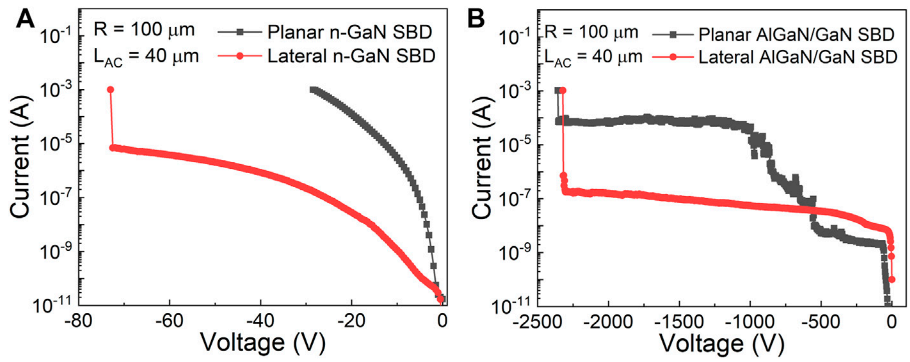

FIGURE 5
Reverse *I-V* characteristics of **(A)** n-GaN SBDs and **(B)** AlGaN/GaN SBDs.

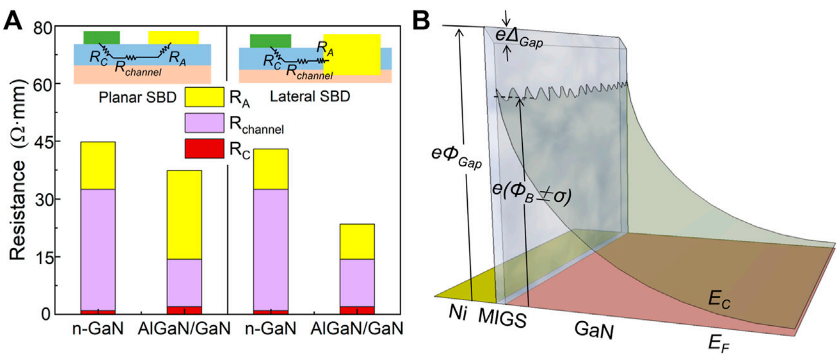

FIGURE 6
(A) Unitized R_{on} distributions in planar and lateral SBDs. **(B)** Energy diagram of n-GaN SBD with MIGS and inhomogeneous SBHs.

larger R_A due to the electrons passing through the AlGaN barrier layer under the anode metal [39].

Conclusion

In summary, the lateral SBDs based on n-GaN and AlGaN/GaN heterostructure were fabricated, and the temperature-dependent *I-V* and *C-V* characteristics were used to evaluate the electrical properties, such as transport mechanisms of the forward and reverse current, SBHs, R_{on} distribution, MIGS, inhomogeneous SBHs, etc. For the planar and lateral n-GaN SBDs, the values of the V_{on} are similar. However, compared with conventional planar AlGaN/GaN SBD, the V_{on} of lateral AlGaN/GaN SBD is reduced from 1.64 V to 0.87 V. The capacitances of lateral n-GaN SBD and lateral AlGaN/GaN SBD are 1.35 pF/mm and 0.70 pF/mm, respectively, which are much smaller than the capacitance of planar SBDs. According to the analysis of inhomogeneous SBHs, etching damage degrades the uniformity of SBHs. Compared with the breakdown voltage of 73 V in the lateral n-GaN SBD, the lateral AlGaN/GaN SBDs exhibit a breakdown voltage of 2322 V. In addition, the R_A is much greater than the R_C due to worsening anode contact by MIGS from the analysis of the R_{on} distributions of each SBD.

Data availability statement

The raw data supporting the conclusions of this article will be made available by the authors, without undue reservation.

Author contributions

Conceptualization: HL and BZ. Investigation: HL, ZL, FW, YX, XY, and YiL. Methodology: HL and BZ. Project administration:

XL, LL, YaL, and ZW. Software: HL and BZ. Validation: HL, ZL, and BZ. Writing—original draft: HL, ZL, and BZ.

Funding

This work was supported by Science and Technology Plan of Guangdong Province, China (Grant Nos. 2019B010132003 and 2019B010132001), the joint funding of the Nature Science Foundation of China (NSFC) and the Macao Science and Technology Development Fund (FDCT) of China (Grant No. 62061160368), the National Key Research and Development Program (Grant Nos. 2016YFB0400105 and 2017YFB0403001), and the Zhuhai Key Technology Laboratory of Wide Bandgap Semiconductor Power Electronics, Sun Yat-sen University, China (Grant No. 20167612042080001).

Conflict of interest

The authors declare that the research was conducted in the absence of any commercial or financial relationships that could be construed as a potential conflict of interest.

Publisher's note

All claims expressed in this article are solely those of the authors and do not necessarily represent those of their affiliated organizations, or those of the publisher, the editors and the reviewers. Any product that may be evaluated in this article, or claim that may be made by its manufacturer, is not guaranteed or endorsed by the publisher.

References

1. Sun Y, Kang X, Zheng Y, Lu J, Tian X, Wei K, et al. Review of the recent progress on GaN-based vertical power Schottky barrier diodes (SBDs). *Electronics* (2019) 8(5):575. doi:10.3390/electronics8050575

2. Mitova R, Ghosh R, Mhaskar U, Klikic D, Wang M-X, Dentella A. Investigations of 600-V GaN HEMT and GaN diode for power converter applications. *IEEE Trans Power Electron* (2014) 29(5):2441–52. doi:10.1109/tpel.2013.2286639

3. Zhang L, Liang S, Lv Y, Yang D, Fu X, Song X, et al. High-power 300 GHz solid-state source chain based on GaN doublers. *IEEE Electron Device Lett* (2021) 42(11):1588–91. doi:10.1109/led.2021.3110781

4. Millan J, Godignon P, Perpina X, Perez-Tomas A, Rebollo J. A survey of wide bandgap power semiconductor devices. *IEEE Trans Power Electron* (2014) 29(5):2155–63. doi:10.1109/tpel.2013.2268900

5. Vurgaftman I, Meyer JR, Ram-Mohan LR. Band parameters for III-V compound semiconductors and their alloys. *J Appl Phys* (2001) 89(11):5815–75. doi:10.1063/1.1368156

6. Pearton SJ, Ren F, Zhang AP, Lee KP. Fabrication and performance of GaN electronic devices. *Mater Sci Eng R: Rep* (2000) 30(3-6):55–212. doi:10.1016/s0927-796x(00)00028-0

7. Ambacher O, Foutz B, Smart J, Shealy JR, Weimann NG, Chu K, et al. Two dimensional electron gases induced by spontaneous and piezoelectric polarization in undoped and doped AlGaN/GaN heterostructures. *J Appl Phys* (2000) 87(1):334–44. doi:10.1063/1.371866

8. Yu ET, Dang XZ, Asbeck PM, Lau SS, Sullivan GJ. Spontaneous and piezoelectric polarization effects in III-V nitride heterostructures. *J Vac Sci Technol B* (1999) 17(4):1742–9. doi:10.1116/1.590818

9. Soni A, Shrivastava M. Design guidelines for recessed Schottky barrier AlN/GaN diode for THz applications. *IEEE Trans Electron Devices* (2021) 68(5):2196–204. doi:10.1109/ted.2021.3064541

10. Shinohara K, Regan DC, Tang Y, Corrion AL, Brown DF, Wong JC, et al. Scaling of GaN HEMTs and Schottky diodes for submillimeter-wave MMIC applications. *IEEE Trans Electron Devices* (2013) 60(10):2982–96. doi:10.1109/ted.2013.2268160

11. Dang K, Wei K, Hao Y, Zhang J, Zhou H, Huang S, et al. A 5.8-GHz high-power and high-efficiency rectifier circuit with lateral GaN Schottky diode for wireless power transfer. *IEEE Trans Power Electron* (2020) 35(3):2247–52. doi:10.1109/tpel.2019.2938769

12. Dang K, Zhang J, Zhou H, Yin S, Zhang T, Ning J, et al. Lateral GaN Schottky barrier diode for wireless high-power transfer application with high RF/DC conversion efficiency: From circuit construction and device technologies to system demonstration. *IEEE Trans Ind Electron* (2020) 67(8):6597–606. doi:10.1109/tie.2019.2939968

13. Zhang T, Zhang J, Zhou H, Zhang Y, Chen T, Zhang K, et al. High-performance lateral GaN Schottky barrier diode on silicon substrate with low turn-on voltage of 0.31 V, high breakdown voltage of 2.65 kV and high-power figure-of-merit of 2.65 GW cm^{-2}. *Appl Phys Express* (2019) 12(4):046502. doi:10.7567/1882-0786/ab0712

14. Zhang Y, Zhang J, Zhou H, Zhang T, Wang H, Feng Z, et al. Leakage current mechanisms of groove-type tungsten-anode GaN SBDs with ultra low turn-on voltage and low reverse current. *Solid State Electron* (2020) 169:107807. doi:10.1016/j.sse.2020.107807

15. Li X, Pu T, Li X, Li L, Ao J-P. Correlation between anode area and sensitivity for the TiN/GaN Schottky barrier diode temperature sensor. *IEEE Trans Electron Devices* (2020) 67(3):1171–5. doi:10.1109/ted.2020.2968358

16. Yao Y, Zhong J, Zheng Y, Yang F, Ni Y, He Z, et al. Current transport mechanism of AlGaN/GaN Schottky barrier diode with fully recessed Schottky anode. *Jpn J Appl Phys* (2015) 54(1):011001. doi:10.7567/jjap.54.011001

17. Li A, Wang C, He Y, Zheng X, Ma X, Zhao Y, et al. GaN-based super-lattice Schottky barrier diode with low forward voltage of 0.81V. *Superlattices Microstruct* (2021) 156:106952. doi:10.1016/j.spmi.2021.106952

18. Waller WM, Gajda M, Pandey S, Uren MJ, Kuball M. Lateral charge distribution and recovery of dynamic R_{on} in AlGaN/GaN HEMTs. *IEEE Trans Electron Devices* (2018) 65(10):4462–8. doi:10.1109/ted.2018.2865037

19. Yang L, Yao W, Liu Y, Wang L, Dai Y, Liu H, et al. Low capacitance AlGaN/GaN based air-bridge structure planar Schottky diode with a half through-hole. *AIP Adv* (2020) 10(4):045219. doi:10.1063/5.0004470

20. Lei Y, Lu H, Cao D, Chen D, Zhang R, Zheng Y. Reverse leakage mechanism of Schottky barrier diode fabricated on homoepitaxial GaN. *Solid State Electron* (2013) 82:63–6. doi:10.1016/j.sse.2013.01.007

21. Yildirim N, Ejderha K, Turut A. On temperature-dependent experimental *I-V* and *C-V* data of Ni/n-GaN Schottky contacts. *J Appl Phys* (2010) 108(11):114506. doi:10.1063/1.3517810

22. Lei W, Nathan MI, Lim TH, Khan MA, Chen Q. High barrier height GaN Schottky diodes: Pt/GaN and Pd/GaN. *Appl Phys Lett* (1996) 68(9):1267–9. doi:10.1063/1.115948

23. Schmitz AC, Ping AT, Asif Khan M, Chen Q, Yang JW, Adesida I. Schottky barrier properties of various metals on n-type GaN. *Semicond Sci Technol* (1996) 11(10):1464–7. doi:10.1088/0268-1242/11/10/002

24. Monch W. Barrier heights of real Schottky contacts explained by metal-induced gap states and lateral inhomogeneities. *J Vac Sci Technol B* (1999) 17(4):1867–76. doi:10.1116/1.590839

25. Tersoff J. Schottky barrier heights and the continuum of gap states. *Phys Rev Lett* (1984) 52(6):465–8. doi:10.1103/PhysRevLett.52.465

26. Tung RT. The physics and chemistry of the Schottky barrier height. *Appl Phys Rev* (2014) 1(1). doi:10.1063/1.4858400

27. Shin J-H, Park J, Jang S, Jang T, Kim KS. Metal induced inhomogeneous Schottky barrier height in AlGaN/GaN Schottky diode. *Appl Phys Lett* (2013) 102(24):243505. doi:10.1063/1.4811756

28. Ren Y, He Z, Dong B, Wang C, Zeng Z, Li Q, et al. Analysis of electrical properties in Ni/GaN Schottky contacts on nonpolar/semipolar GaN free-standing substrates. *J Alloys Compd* (2022) 898:162817. doi:10.1016/j.jallcom.2021.162817

29. Iucolano F, Roccaforte F, Giannazzo F, Raineri V. Barrier inhomogeneity and electrical properties of Pt/GaN Schottky contacts. *J Appl Phys* (2007) 102(11): 113701. doi:10.1063/1.2817647

30. Werner JH, Guttler HH. Barrier inhomogeneities at Schottky contacts. *J Appl Phys* (1991) 69(3):1522–33. doi:10.1063/1.347243

31. Wu M, Zheng D-Y, Wang Y, Chen W-W, Zhang K, Ma X-H, et al. Schottky forward current transport mechanisms in AlGaN/GaN HEMTs over a wide temperature range. *Chin Phys B* (2014) 23(9):097307. doi:10.1088/1674-1056/23/9/097307

32. Benamara Z, Akkal B, Talbi A, Gruzza B. Electrical transport characteristics of Au/n-GaN Schottky diodes. *Mater Sci Eng C* (2006) 26(2-3):519–22. doi:10.1016/j.msec.2005.10.016

33. Reddy MSP, Kumar AA, Reddy VR. Electrical transport characteristics of Ni/Pd/n-GaN Schottky barrier diodes as a function of temperature. *Thin Solid Films* (2011) 519(11):3844–50. doi:10.1016/j.tsf.2011.01.258

34. Yan D, Jiao J, Ren J, Yang G, Gu X. Forward current transport mechanisms in Ni/Au-AlGaN/GaN Schottky diodes. *J Appl Phys* (2013) 114(14):144511. doi:10.1063/1.4824296

35. Roccaforte F, Giannazzo F, Alberti A, Spera M, Cannas M, Cora I, et al. Barrier inhomogeneity in vertical Schottky diodes on free standing gallium nitride. *Mater Sci Semicond Process* (2019) 94:164–70. doi:10.1016/j.mssp.2019.01.036

36. Shao Z, Chen D, Lu H, Zhang R, Cao D, Luo W, et al. High-gain AlGaN solar-blind avalanche photodiodes. *IEEE Electron Device Lett* (2014) 35(3):372–4. doi:10.1109/LED.2013.2296658

37. Wen Q, Wang C, Qiu X, Lv Z, Jiang H. Significant performance improvement of AlGaN solar-blind heterojunction phototransistors by using Na_2S solution based surface treatment. *Appl Surf Sci* (2022) 591:153144. doi:10.1016/j.apsusc.2022.153144

38. Zhang H, Miller EJ, Yu ET. Analysis of leakage current mechanisms in Schottky contacts to GaN and $Al_{0.25}Ga_{0.75}N$/GaN grown by molecular-beam epitaxy. *J Appl Phys* (2006) 99(2):023703. doi:10.1063/1.2159547

39. Cao Z-F, Lin Z-J, Lu Y-J, Luan C-B, Yu Y-X, Chen H, et al. Determination of the series resistance under the Schottky contacts of AlGaN/AlN/GaN Schottky barrier diodes. *Chin Phys B* (2012) 21(1):017103. doi:10.1088/1674-1056/21/1/017103